Natural orbitals and Bose-Einstein condensates in traps: A diffusion Monte Carlo analysis

J. L. DuBois and H. R. Glyde
Department of Physics and Astronomy, University of Delaware, Newark, Delaware 19716, USA
(Received 21 March 2003; published 10 September 2003)

We investigate the properties of hard-core bosons in harmonic traps over a wide range of densities. Bose-Einstein condensation is formulated using the one-body density matrix (OBDM) which is equally valid at low and high densities. The OBDM is calculated using diffusion Monte Carlo methods and it is diagonalized to obtain the ''natural'' single-particle orbitals and their occupation, including the condensate fraction. At low boson density, $na^3<10^{-5}$, where $n=N/V$ and a is the hard-core diameter, the condensate is localized at the center of the trap. As na^3 increases, the condensate moves to the edges of the trap. At high density, it is localized at the edges of the trap. At $na^3\leqslant 10^{-4}$, the Gross-Pitaevskii theory of the condensate describes the whole system within 1%. At $na^3\approx 10^{-3}$, corrections are 3% to the Grass-Pitaevskii energy but 30% to the Bogoliubov prediction of the condensate depletion. At $na^3\gtrsim 10^{-2}$, mean-field theory fails. At $na^3\gtrsim 0.1$, the bosons behave more like a liquid ^{4}He droplet than a trapped boson gas.

DOI: 10.1103/PhysRevA.68.033602 PACS number(s): 03.75.Hh, 03.75.Gg, 03.75.Nt

I. INTRODUCTION

Bose-Einstein condensation (BEC) has been a topic of fundamental interest since it was first predicted by Einstein in 1924 [1]. He showed that as a consequence of Bose statistics [2] a macroscopic fraction N_0/N of the atoms in an ideal Bose gas can condense into a single quantum state. London [3,4] postulated that superfluidity in liquid ^{4}He was a consequence of a transition to BEC. But liquid ^{4}He is a strongly interacting, dense Bose liquid and the connection between BEC in an ideal gas and superfluidity was not at all clear [5]. Similarly, the many-body correlation effects induced by the interboson interaction significantly reduce the condensate fraction even at zero temperature [6,7]. Modern direct measurements [8] of BEC in liquid ^{4}He find only 7.25% of the liquid in the condensate at $T=0$ K.

The theoretical framework for treating an interacting Bose gas was initiated in 1947 by Bogoliubov [9]. He developed a perturbation expansion valid for low density and weak interaction, $na^3\ll 1$ (where n is the number density N/V and a is the hard-core diameter of the bosons), and small depletion of the condensate, $(N-N_0)/N\ll 1$. About a decade later, Onsager and Penrose [10] and Löwdin [11] formulated a definition of BEC in terms of the eigenvalues and eigenvectors (natural orbitals) of the one-body density matrix (OBDM). An orbital with macroscopic occupation arising from diagonalization of the OBDM is defined as the ''condensate wave function'' or order parameter. This formulation allows direct access to condensate properties at arbitrary density and does not require a large condensate fraction. The work in this paper is based on the OBDM formulation of BEC which is rigorously valid for a strongly interacting system [5].

In 1995, experiments in weakly interacting dilute vapors of the alkali-metal atoms ^{87}Rb, ^{23}Na, and ^{7}Li in magnetic traps provided direct evidence of a clear transition from a thermally distributed cloud to macroscopic occupation of a single quantum state [12–14]. This long awaited direct realization of BEC spawned a dramatic renewal of interest in Bose systems and BEC. Since the densities in these experiments were low (typical number densities were 10^{12} cm^{-3} and $na^3\approx 10^{-6}$, where a is the s-wave scattering length of the atoms), almost all of the theoretical activity has focused on the weakly interacting gas limit and the Gross-Pitaevskii (GP) equation [15]. The GP equation provides an excellent mean-field description of the condensate at low density. This is a valid description of the whole Bose gas in the dilute limit, $na^3\ll 1$, where most of the atoms are in the condensate. However, it is inaccurate for strongly interacting systems in which the condensate fraction is significantly depleted by quantum fluctuations. Since the experiments in 1995, only a handful of studies have attempted to consider the properties of BEC beyond the dilute regime and the GP description of the condensate [16–37]. Most of this relatively small body of work rely on modified forms of the GP equation which incorporate higher terms in the Bogoliubov expansion that include effects of atoms outside the condensate within a local-density approximation. Unfortunately, the condensate fraction and distribution in the trap calculated by such methods become inaccurate as the density becomes greater than $na^3\gtrsim 10^{-3}$ [25].

It has recently become possible to study Bose systems with tunable interactions [38–43] for which densities of up to $na^3\approx 1$ are obtainable. Specifically, ^{85}Rb at densities in the range $na^3\approx 10^{-3}-10^{-1}$ has been investigated. BEC in metastable helium isotopes [44–46] with $na^3\approx 10^{-4}$ and in atomic hydrogen [47] with $na^3\approx 10^{-5}$, are also higher-density Bose gases. This makes the study of BEC and the role of interactions in trapped Bose gases over a wide range of densities of direct interest to experiment.

The chief purpose of this work is to go beyond the dilute limit, to test the limits of the GP equation and related mean-field approximations and to explore the zero-temperature properties of trapped hard-core bosons as na^3 increases from the dilute limit to the dense regime corresponding to liquid ^{4}He, and beyond. The range of densities investigated here is displayed in Fig. 1. We increase the density by increasing both N and the hard-core diameter a up to the value $na^3\simeq 0.21$ which describes liquid ^{4}He at saturated vapor pressure (SVP) when the ^{4}He atoms are represented by hard

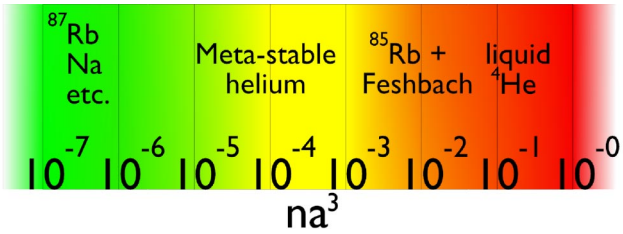

FIG. 1. Range of system densities considered in this work expressed in terms of $na^3 \equiv Na^3/V$, the ratio of the volume occupied by N hard-core particles with diameter a to the total volume of the system V.

spheres of diameter $a=2.203$ Å [48]. The ground-state energy E, the total density distribution, and the OBDM are evaluated using diffusion Monte Carlo (DMC) methods.

Specifically, we compare the ground-state energy of the whole trapped gas calculated using DMC, E_{DMC}, with the usual energy of the condensate calculated using the GP equation, E_{GP}. As density increases, E_{DMC} and E_{GP} begin to differ. For example, at $na^3=10^{-3}$, we find $(E_{DMC}-E_{GP})/E_{GP}=3\%$. Modified GP equations provide a mean-field description of the atoms above the condensate. The dependence of $E_{DMC}-E_{GP}$ on the number of trapped bosons N and on the scattering length a follows the predictions of the modified GP equation remarkably well up to high densities, $na^3 \approx 5\times 10^{-2}$. This suggests that the difference $E_{DMC}-E_{VMC}$ (where VMC densities variational Monte Carlo) can be attributed to the atoms above the condensate. However, the energy is not as sensitive to approximations as some other properties.

We compare the condensate fraction obtained using the rigorous OBDM-DMC method with predictions of the Bogoliubov theory. The two agree within 1% for $na^3 \lesssim 10^{-4}$. At higher densities, the Bogoliubov theory significantly underestimates the depletion of the condensate, by 25% at $na^3 \approx 2\times 10^{-2}$. We evaluate the condensate density distribution in the trap. At low density, the condensate is localized at the center of the trap as usually found [15]. At higher density $(na^3 \approx 10^{-2})$, the condensate is spaced over several trap lengths and the condensate and total density have similar distributions. Also, at higher densities $(na^3 \gtrsim 2\times 10^{-2})$, oscillations in the total density distribution appear which are not found in mean-field theories. There are no corresponding oscillations in the condensate density distribution. At high density $(na^3 \gtrsim 0.10)$, the condensate is localized at the edges of the trap (large r/a) where the total boson density is low. At high density, the trapped bosons resemble liquid-^{4}He droplets [49–51].

We also compare the present DMC results with our earlier variational Monte Carlo values [50]. We find that the VMC and DMC energies agree well at all densities and that the ground-state energy is not very sensitive to the trial variational wave function. However, the OBDM and the condensate fraction is very sensitive to the trial wave function at higher densities. An accurate initial trial function is needed to get reliable condensate fractions even in the DMC formulation.

Monte Carlo methods are usually applied to dense systems such as liquid and solid ^{4}He [6,7]. Recently, Giorgini *et al.* have evaluated the energy and condensate fraction of the uniform Bose gas over a wide density range, $10^{-6} \leqslant na^3 \leqslant 10^{-3}$ [25]. Grüter *et al.* [20] have evaluated the critical temperature T_c for BEC in a Bose gas using path-integral Monte Carlo (PIMC) methods. They find T_c is increased above the ideal Bose gas value by interaction in the dilute range. This increase is observed in dilute concentrations of ^{4}He in Vycor [52]. At liquid-^{4}He densities, T_c is decreased by interaction [53,54].

Krauth [16] first applied QMC (quantum Monte Carlo) to BEC in a trap using PIMC methods. For 10 000 hard-sphere bosons in a spherical trap with a ratio of hard-core diameter to trap length, $a/a_{ho}=4.3\times 10^{-3}(na^3 \approx 10^{-4})$, he found that condensate was concentrated at the center of the trap while the uncondensed atoms were spread over a wide range and well described by a classical Bose gas. Holzmann and Krauth [22] made a direct comparison of PIMC and Hartree-Fock calculations for a dilute gas of hard spheres in a trap with $a/a_{ho}=4.3\times 10^{-3}$. For temperatures near T_c, they found N_0 was greater in PIMC. The increase in N_0 with exact representation of the interaction effects is consistent with the corresponding increase in T_c with interaction in the uniform Bose gas.

Recently, QMC methods have been successfully applied to the study of highly inhomogeneous Bose systems. Astrakharchik *et al.* used DMC to study BEC and superfluidity in a Bose gas with disorder at zero temperature [31]. They find an intriguing decoupling of the superfluid and condensate fractions for strong disorder. Studies of superfluid ^{4}He with a free surface [27,33] found the local condensate fraction peaks $(n_0 \approx 0.95\%$ [33]) in the dilute region just inside the liquid-vacuum interface. Blume [36] and Astrakharchik and Giorgini [37] have examined the transition from the three-dimensional to the quasi-one-dimensional regime for bosons in highly elongated cigar-shaped traps. They confirm that the Bose gas undergoes ''fermionization'' in the quasi-1D regime.

In Sec. II, we describe the theoretical framework and computational methods used. Section III contains the present results. In Sec. IV, the chief results are reviewed and discussed.

II. METHODS

We consider N bosons of mass m confined in an external trapping potential $V_{ext}(\mathbf{r})$ and interacting via a two-body potential $V_{int}(\mathbf{r}_1,\mathbf{r}_2)$. The Hamiltonian for this system is

$$H=\sum_i^N \left(\frac{-\hbar^2}{2m}\nabla_i^2+V_{ext}(\mathbf{r}_i)\right)+\sum_{i<j}^N V_{int}(\mathbf{r}_i,\mathbf{r}_j). \qquad (1)$$

Here,

$$V_{ext}(\mathbf{r})=\tfrac{1}{2}m\omega_{ho}^2 r^2, \qquad (2)$$

where ω_{ho}^2 is the characteristic trap frequency. Interactions are modeled by a hard-sphere potential

$$V_{int}(r)=\begin{cases}\infty, & r\leqslant a\\ 0, & r>a.\end{cases} \tag{3}$$

Introducing lengths in units of the characteristic trap length $a_{ho}=(\hbar/m\omega_{ho})^{1/2}$, $r\rightarrow r/a_{ho}$, and energies in units of $\hbar\omega_{ho}$ as in Ref. [15], the many-body Hamiltonian is

$$H=\sum_{i}^{N}\frac{1}{2}(-\nabla_i^2+r_i^2)+\sum_{i<j}V_{int}(|\mathbf{r}_i-\mathbf{r}_j|). \tag{4}$$

A. Diffusion Monte Carlo implementation

Diffusion Monte Carlo is a method for finding the exact properties of the quantum-mechanical ground state of a many-body system to within arbitrary precision—see, for example, Ref. [55]. The starting point for this method is the time-dependent Schrödinger equation in imaginary time:

$$\left[-\frac{\hbar^2}{2m}\nabla^2+V(\mathbf{R})-E_T\right]\Psi(\mathbf{R},t)=-\hbar\frac{\partial\Psi(\mathbf{R},t)}{\partial t}. \tag{5}$$

The time-dependent component of $\Psi(\mathbf{R},t)$, $Q_i(t)$, is $Q_i(t)=\exp[-(E_i-E_T)t/\hbar]$. E_T is an adjustable target energy. In the $t\rightarrow\infty$ limit, the steady-state solution of Eq. (5) is the ground state $\Phi_0(\mathbf{R})$.

The term diffusion Monte Carlo comes from the resemblance of Eq. (5) to the classic diffusion equation

$$D\nabla^2\rho(\mathbf{R},t)=\frac{\partial\rho(\mathbf{R},t)}{\partial t}. \tag{6}$$

This equation can be simulated by a Monte Carlo random walk in configuration space. Treating the $[V(\mathbf{R})-E_T]\Psi(\mathbf{R},t)$ component of Eq. (5) alone results in a rate equation of the form

$$v(\mathbf{R})\rho(\mathbf{R},t)=-\frac{\partial\rho(\mathbf{R},t)}{\partial t}. \tag{7}$$

This component represents a branching process in which the growth or decay of a population is proportional to its density. In the present implementation the diffusion and branching processes are combined to simulate Eq. (5) and obtain the zero-temperature ground state of the time-independent Schrödinger equation.

A simple application of Eq. (5) above results in a branching rate which is proportional to the potential energy $V(\mathbf{R})-E_T$. This means that large fluctuations in the potential $V(\mathbf{R})$ will cause correspondingly large fluctuations in the population of walkers. Dramatic fluctuations in the number of walkers can result in large inefficiencies when treating realistic many-body systems. The solution to this problem was first presented by Kalos *et al.* [48]. In this method, a trial function is introduced to *guide* the metropolis walk to regions of higher probability and lower potential energy resulting in lower fluctuations in the population of walkers. The wave function in Eq. (5) is replaced by a product of the true ground state $\Psi(\mathbf{R},t)$ and a guiding function $\Psi_T(\mathbf{R})$:

$$\Psi(\mathbf{R},t)\rightarrow\Psi(\mathbf{R},t)\Psi_T(\mathbf{R}). \tag{8}$$

While use of a guiding function is necessary for the efficient application of the DMC method, it can introduce a bias into the calculation of observables which do not commute with the Hamiltonian unless corrective measures are taken—such as the application of ''forward walking'' [48,56].

We evaluate the expectation value $\langle\Psi|O|\Psi\rangle$ of an operator O, using QMC. In integral form the expectation value is

$$\langle\Psi|O|\Psi\rangle=\int d\mathbf{R}\Psi^*(\mathbf{R})O(\mathbf{R})\Psi(\mathbf{R}). \tag{9}$$

To evaluate this expression using QMC, Eq. (9) is recast as

$$\langle\Psi|O|\Psi\rangle=\int d\mathbf{R}|\Psi(\mathbf{R})|^2\left[\frac{O(\mathbf{R})\Psi(\mathbf{R})}{\Psi(\mathbf{R})}\right]. \tag{10}$$

The result of a QMC calculation is a set of configurations $\{\mathbf{R}_1,\ldots,\mathbf{R}_M\}$ sampled from $|\Psi|^2$. Using these configurations we may estimate $\langle\Psi|O|\Psi\rangle$ as

$$\langle\Psi|O|\Psi\rangle\approx\frac{1}{M}\sum_{i=1}^{M}\frac{O(\mathbf{R}_i)\Psi(\mathbf{R}_i)}{\Psi(\mathbf{R}_i)}. \tag{11}$$

This estimate becomes exact as $M\rightarrow\infty$.

B. The OBDM and natural orbitals

A goal in this work is to describe BEC in systems with interactions. To do this we require a definition of the condensate single-particle state. Following Onsager and Penrose, and Löwdin [10,11], we take OBDM as the fundamental quantity for an interacting system and define the natural single-particle orbitals (NO) in terms of the OBDM. The OBDM is [57]

$$\rho(\mathbf{r}',\mathbf{r})=\langle\hat{\Psi}^\dagger(\mathbf{r}'),\hat{\Psi}(\mathbf{r})\rangle, \tag{12}$$

where $\hat{\Psi}(\mathbf{r})$ is the field operator that annihilates a single particle at the point $\mathbf{r}$ in the system. To define the NO, we introduce a set of single-particle states having wave functions $\phi_i(\mathbf{r})$ and expand $\hat{\Psi}(\mathbf{r})$ in terms of these states and the operators $\hat{a}_i$ which annihilate a particle from $|i\rangle$,

$$\hat{\Psi}=\sum_i\phi_i(\mathbf{r})\hat{a}_i. \tag{13}$$

Requiring that the $\hat{a}_i$ satisfy the usual commutation $([\hat{a}_i^\dagger,\hat{a}_j]=\delta_{ij})$ and number relations $(\langle\hat{a}_i^\dagger\hat{a}_j\rangle=N_i\delta_{ij})$, we have

$$\rho(\mathbf{r},\mathbf{r}')=\sum_{ij}\phi_j^*(\mathbf{r}')\phi_i(\mathbf{r})N_i\delta_{ij}=\sum_{ij}\phi_j^*(\mathbf{r})\phi_i(\mathbf{r}')N_i\delta_{ij}. \tag{14}$$

This may be taken as the defining relation of the NO, $\phi_i(\mathbf{r})$. Specifically, we have from Eq. (14),

$$\int d\mathbf{r}d\mathbf{r}'\,\phi_i^*(\mathbf{r})\rho(\mathbf{r},\mathbf{r}')\phi_j(\mathbf{r}')=N_i\delta_{ij}, \tag{15}$$

so that the NO may be obtained by diagonalizing the OBDM. The eigenvectors are the NO and the eigenvalues are the occupation N_i of the orbitals. In principle any orbital which satisfies $N_i \gg 1$ may be considered a macroscopically occupied pseudoparticle state—i.e., the equivalent of a Bose-Einstein condensate. A Bose system with more than one macroscopically occupied state would represent a fragmented condensate [5]. In the systems studied in this work, only a single condensate orbital was found to have macroscopic occupation. The condensate is therefore the orbital having the highest occupation, denoted by $\phi_0(r)$, and the condensate fraction is $n_0=N_0/N$.

Relations (14) and (15) involve the vector $\mathbf{r}$ and $\mathbf{r}'$ and cannot be solved directly as matrix equations. To obtain matrix equations, we restrict ourselves to spherical traps and seek equations for the radial component of the NO as in Ref. [50]. In this approach, the OBDM is expanded in Legendre Polynomials $P_l(\hat{\mathbf{r}}_1\cdot\hat{\mathbf{r}}_1')$ and evaluated using the QMC ground state Ψ_0 as

$$\rho_l(r_1,r_1')=\int d\Omega_1 d\mathbf{r}_2\cdots d\mathbf{r}_N\Psi_0^*(\mathbf{r}_1\cdots\mathbf{r}_N) \times P_l(\hat{\mathbf{r}}_1\cdot\hat{\mathbf{r}}_1')\Psi_0(\mathbf{r}_1'\cdots\mathbf{r}_N). \tag{16}$$

C. QMC evaluation of $\rho_l(r,r')$

In QMC we evaluate Eq. (16) in a form similar to Eq. (10) giving

$$\rho_l(r_1,r_1')\approx\frac{1}{4\pi\epsilon}\int_{r_1-\epsilon/2}^{r_1+\epsilon/2}dr_1\int d\Omega_1 d\tilde{\mathbf{R}}|\Psi(\mathbf{r}_1,\tilde{\mathbf{R}})|^2 \times\left[\frac{P_l(\hat{r}_1\cdot\hat{r}_1')\Psi(\mathbf{r}_1',\tilde{\mathbf{R}})}{\Psi(\mathbf{r}_1,\tilde{\mathbf{R}})}\right], \tag{17}$$

where $\tilde{\mathbf{R}}\equiv(\mathbf{r}_2,\ldots,\mathbf{r}_N)$ and ϵ is the width of the grid elements upon which $\rho_l(r_1,r_1')$ is being evaluated. Because the systems we are evaluating are spherically symmetric, the direction of $\mathbf{r}'$ is arbitrary. We may take advantage of this fact to reduce the statistical uncertainty in estimates of $\rho_l(r,r')$ by evaluating Eq. (17) for several different directions of $\mathbf{r}'$ and taking the average result. In addition, since we are dealing with identical bosons, the OBDM does not depend on the particle being evaluated so $\rho_l(r_1,r_1')=\rho_l(r_i,r_i')$. This allows us to take the average, $\rho_l(r_1,r_1')=1/N\Sigma_i\rho_l(r_i,r_i')$.

D. Diagonalization and error estimation

Using the method described above, the OBDM is evaluated on a grid of values of $r=i\epsilon$ and $r'=j\epsilon$, where i and j are integers in the range $0\leq i,j\leq Q$ (where Q is a maximum cutoff). We may then construct the discreet matrix $[i\epsilon\rho_l(i\epsilon,j\epsilon)j\epsilon]$, which is readily diagonalized by standard matrix diagonalization methods.

Replacing the continuous matrix $\rho_l(r,r')$ with the discreet matrix $[i\epsilon\rho_l(i\epsilon,j\epsilon)j\epsilon]$ is a potential source of systematic error. To avoid this problem, we evaluated each system with decreasing values of the grid spacing ϵ such that $\epsilon_{q+1}=\epsilon_q/2$. The largest value of ϵ for which no significant change in the calculated orbitals and occupation numbers occurred between ϵ_q and ϵ_{q+1} was then used to determine the condensate properties for that system.

A second potential source of error arises in treating $\rho_l(r,r')$ (which is an infinite matrix) as a finite matrix. Since the trapped systems are spatially finite, the probability of finding a particle beyond the average radius R of the cloud goes to zero very quickly. For the same reason, $\rho_l(r,r')\approx 0$ when either $r>R$ or $r'>R$. It is therefore, safe to treat $\rho_l(r,r')$ as a finite matrix. As a brute force test of this assertion, we evaluated several systems with increasingly large cutoff values. We found no significant change in condensate properties calculated from a OBDM where $r,r'\leq R$ and $r,r'\leq 2R$.

The statistical error associated with a given orbital and its occupation are obtained as follows. When the initial OBDM, ρ^0, is calculated the variance associated with each matrix element in ρ^0 is obtained. The original ρ^0 is assumed to represent a randomly sampled event from a Gaussian error distribution surrounding the true OBDM. Based on this assertion, a set of M new OBDM's, $\{\tilde{\rho}^1\cdots\tilde{\rho}^M\}$, are then generated by allowing each matrix element to randomly vary according to its statistical error. Each of the new OBDM, $\tilde{\rho}^q$, are diagonalized to obtain their corresponding eigenvalues $\tilde{n}_i^q$ and eigenvectors $\tilde{\phi}_i^q$. An average occupation, $\overline{n_i}=1/M\Sigma_q^M\tilde{n}_i^q$, and orbital, $\overline{\phi_i}=\Sigma_q^M\tilde{\phi}_i^q$, are then obtained. The variance of these averages is then used as an estimate of the statistical error of the orbitals and occupation numbers of ρ^0.

III. RESULTS

A. DMC energy

Figure 2 shows the energy per particle calculated by diffusion Monte Carlo, E_{DMC}, by variational Monte Carlo (using the simple trial function of Ref. [50]), E_{VMC0}, and using the Gross-Pitaevskii equation, E_{GP}, of trapped hard-core bosons as a function of maximum density, na^3, in the trap. In the dilute regime, $na^3\lesssim 10^{-4}$, E_{DMC}, E_{VMC0}, and E_{GP} are nearly indistinguishable. The difference in energy at $na^3=5\times10^{-5}$ is, for example, $10^{-3}\hbar\omega_{ho}$ which is within the error bars of the QMC calculations. At higher densities, the DMC energy lies above the GP result by 3% at $na^3=10^{-3}$. E_{VMC0} agrees well with the DMC results with a difference of only 0.3% at $na^3=10^{-3}$.

Figure 3 shows the percent difference between E_{DMC} and E_{GP}, $\delta E/E_{GP}=(E_{DMC}-E_{GP})/E_{GP}$ for $N=128$ hard-sphere bosons in a spherically symmetric harmonic trap at higher densities, na^3. Here, and throughout this paper, GP energies are calculated using a self-interaction term proportional to $(N-1)a/a_{ho}$. GP results using Na/a_{ho} significantly overestimate the energy for small N. The difference between DMC and GP energies is well described by

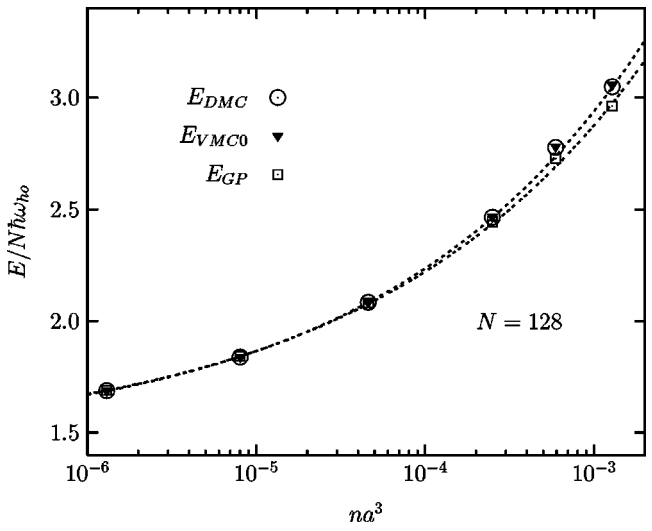

FIG. 2. Diffusion Monte Carlo E_{DMC}, variational Monte Carlo E_{VMC0}, and Gross-Pitaevskii E_{GP}, energies for trapped hard-sphere bosons as a function of maximum density na^3 in the trap. Density is varied by changing scattering length a, $4.3\times10^{-3} < a/a_{ho} < 0.14$, where a_{ho} is the trap length. At higher densities E_{DMC} clearly lies above E_{GP}, 3% at $na^3 = 10^{-3}$. E_{VMC} and E_{DMC} differ by 0.3% at $na^3 = 10^{-3}$.

$\delta E/E_{GP} \propto (na^3)^{2/3}$. This dependence holds even up to trap densities of $na^3 \approx 0.32$, well above the density of liquid helium ($na^3 \approx 0.21$). At this density, E_{GP} and E_{DMC} differ by as much as 80%.

In Fig. 4, the dependence of $\delta E/E_{GP}$ on the scattering length a for $N = 128$ bosons in a spherically symmetric harmonic trap is shown. The figure shows good agreement with $\delta E \propto (a/a_{ho})^{8/5}$. This is precisely the power-law relation predicted by the first-order correction to the Gross-Pitaevskii

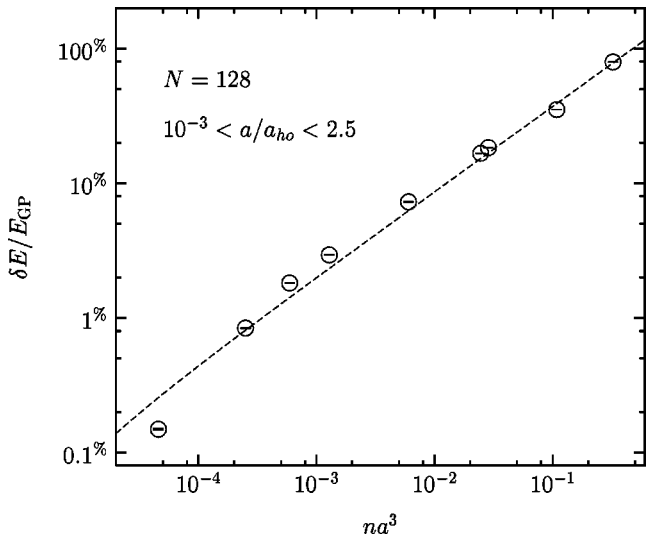

FIG. 3. Percent difference between diffusion Monte Carlo E_{DMC} and Gross-Pitaevskii E_{GP} energies for hard-core bosons in a spherically symmetric harmonic trap as a function of maximum density na^3 in the trap. The percent difference between DMC and GP energies is well described by $\delta E/E_{GP} \propto (na^3)^{2/3}$ (dashed line).

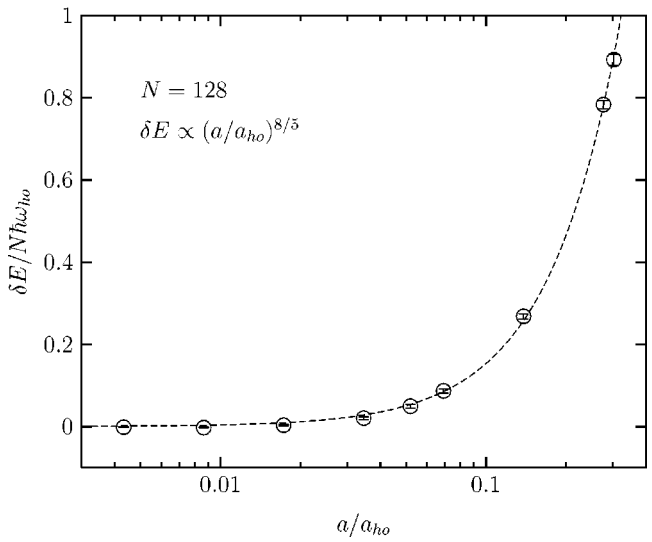

FIG. 4. Dependence of $\delta E = (E_{DMC} - E_{GP})$ on the ratio of the scattering length a to the trap length, $a_{ho} = (\hbar/m\omega_{ho})^{1/2}$, for $N = 128$ bosons in a spherically symmetric harmonic trap. The dashed line shows $\delta E/E_{GP} \propto (a/a_{ho})^{8/5}$.

energy which takes into account particles above the condensate, denoted the modified Gross-Pitaevskii (MGP) equation energy [15].

Figure 5 shows the dependence of $\delta E = E_{DMC} - E_{GP}$ on the number of particles N in the trap. In this plot, the ratio of the scattering length to the characteristic length of the trap is $a/a_{ho} = 8(a_{Rb}/a_{ho}) = 0.034\,64$. The resulting range of densities at the center of the trap lie between $na^3 \approx 8\times10^{-5}$ for $N = 16$ and $na^3 \approx 6\times10^{-4}$ for $N = 1024$. The DMC energy is $\approx 2\%$ higher than the GP energy when $N = 1024$. The dashed line is a least squares fit of δE to a function of the form $q(N) = q_0 + q_1 N^{3/5}$. The relation $\delta E(N) \propto N^{3/5}$ is again consistent with the result obtained from the modified Gross-Pitaevskii equation.

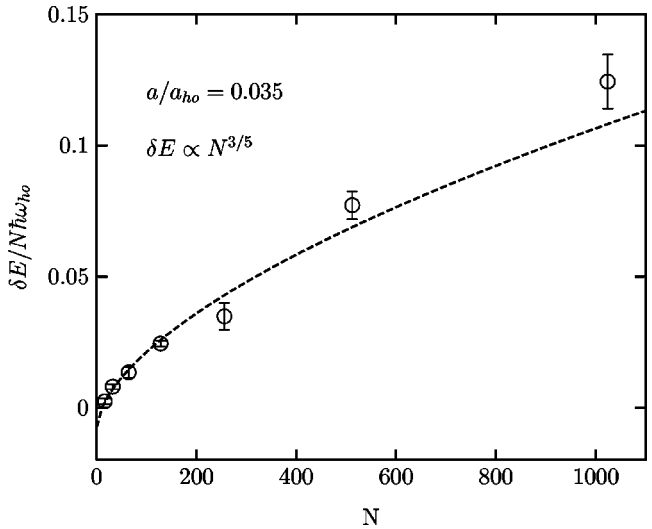

FIG. 5. Dependence of $\delta E = E_{DMC} - E_{GP}$ on the number of particles N in units of $\hbar\omega_{ho}$, where the ratio of the scattering length to the characteristic length of the trap is $a/a_{ho} = 0.034\,64$. The dashed line is $\delta E \propto N^{3/5}$.

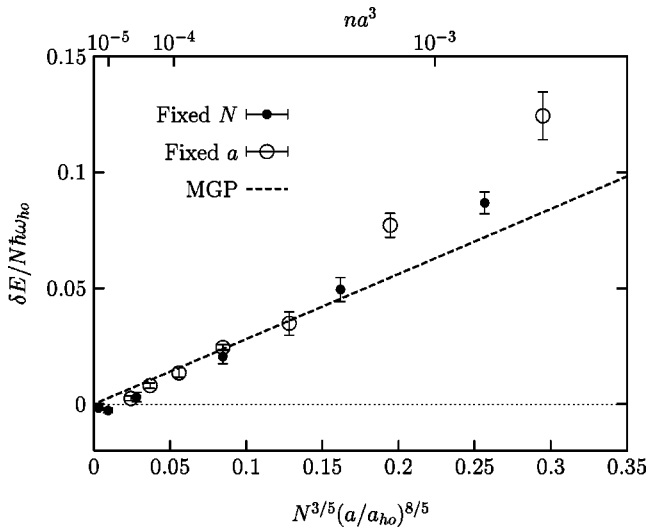

FIG. 6. $\delta E=(E_{DMC}-E_{GP})$ as a function of $N^{3/5}(a/a_{ho})^{8/5}$ for fixed number of particles, $N=128$ (filled circles), and fixed scattering length, $a/a_{ho}=8a_{Rb}$ (open circles), along with the MGP prediction (heavy-dashed line). Values of the maximum trap density na^3 for the fixed N case are shown on the top axis.

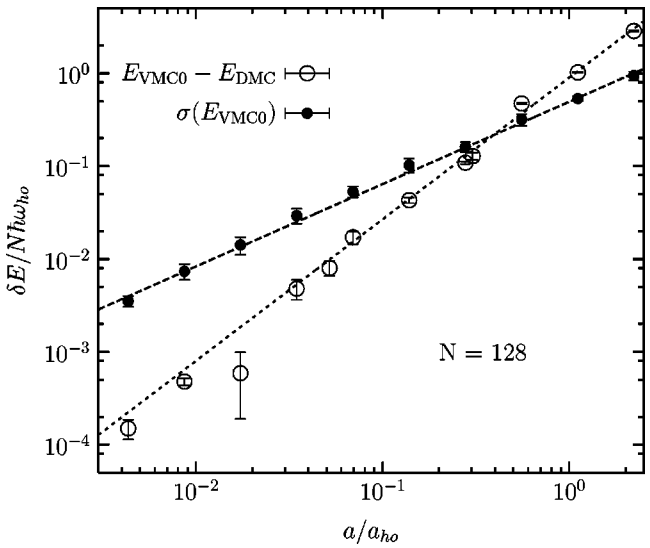

FIG. 7. Difference between DMC and VMC0 energies ($E_{VMC0}-E_{DMC}$) compared with the variance of the VMC0 calculation, $\sigma(E_{VMC0})$, as a function of the ratio of the hard-sphere diameter to the trap length a/a_{ho}.

The MGP expression for the ground-state energy provides the first correction to the GP energy arising from contributions of the noncondensate. If this correction is relevant across the entire range of systems considered, combining the results for the dependence of δE on N and a/a_{ho} as presented in Figs. 4 and 5 should provide a single coefficient ξ such that

$$\delta E=\xi N^{3/5}(a/a_{ho})^{8/5}. \tag{18}$$

MGP predicts $\xi=5(15)^{3/5}/(64\sqrt{2})\approx 0.28$. In Fig. 6, the fixed a and fixed N results are shown together along with the MGP prediction for the first-order contribution to the ground-state energy of atoms depleted from the condensate. The figure demonstrates that for systems with $na^3\lesssim 5\times 10^{-4}$, MGP provides a good description of the DMC corrections to the GP energy. At higher densities, while the fixed a and fixed N results are separately well described by $(a/a_{ho})^{8/5}$ and $N^{3/5}$, respectively, they do not share a common coefficient ξ. This suggests that at higher densities corrections to the condensate energy have a more complicated dependence on N and a than Eq. (18).

B. Range of validity of VMC0 results

To investigate the range of validity of the VMC0 trial function we evaluated the variance of the Hamiltonian. If the trial function is an exact representation of an eigenstate of the Hamiltonian the variance is zero. Figure 7 provides a comparison of the difference between DMC and VMC0 results for the energy per boson, $(E_{VMC0}-E_{DMC})$, and the variance of the energy per boson, $\sigma(E_{VMC0})$, as a function of the ratio of the hard-sphere diameter to the trap length a/a_{ho}. Results are for $N=128$ hard-core bosons in a spherically symmetric trap. Up to a value of $a/a_{ho}\approx 0.3$, the DMC and VMC0 energies agree to within the variance of E_{VMC0}. The maximum density of the trapped bosons for this "critical" value of $a/a_{ho}=0.3$ is $na^3\approx 3\times 10^{-2}$. This indicates that for systems with $na^3\lesssim 10^{-2}$ the VMC0 trial function not only provides a valid upper bound on the energy but a valid lower bound as well.

C. Spatial distribution of trapped bosons

The spatial distribution of trapped bosons is a property which is accessible to experimental observation. The first observations of BEC used the difference between a classical Boltzmann distribution and a condensate distribution as evidence for the existence of BEC [12–14]. Spatial resolution in most observations to date is, however, not very high [typically only $O(10^{-1})$ times the size of the condensate itself] [12,42]. In this section, we compare the present QMC results for the density of the many-body ground state, $n(r)$, with predictions of mean-field theory for the spatial distribution of the condensate, $n_0(r)$. While this comparison is not always strictly correct, since depletion of the condensate means $n(r)\neq n_0(r)$, what is actually observed in experiments is the "total" density which includes condensate and noncondensate atoms alike. The condensate distribution and "total" density have been treated as identical in the analysis of experimental results [40]. For this reason, we will compare $n(r)$ and mean-field results for $n_0(r)$ as if they are indeed measurements of the same physical quantity.

1. The "width" of a trapped cloud of bosons

The radius of the condensate as predicted by the Gross-Pitaevskii equation in the Thomas-Fermi limit ($Na\gg 1$, $a/a_{ho}\ll 1$) is [15]

$$R_{TF}=a_{ho}\left(15N\frac{a}{a_{ho}}\right)^{1/5}. \tag{19}$$

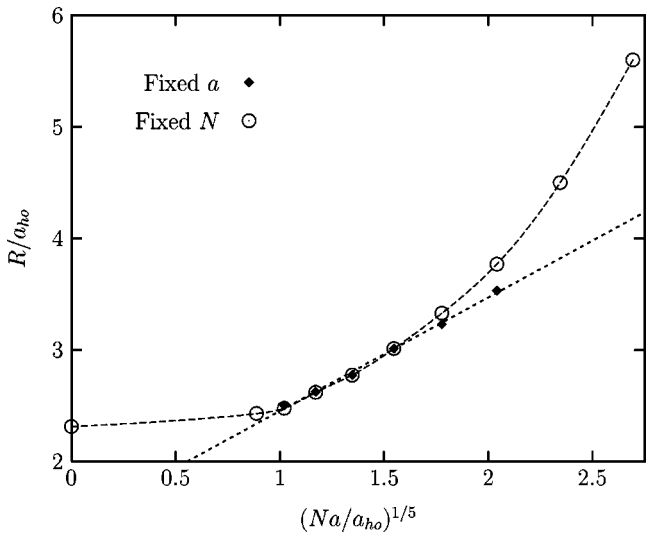

FIG. 8. QMC values of the width R of the ground-state density of hard-core bosons in a harmonic trap vs $(Na/a_{ho})^{1/5}$, where N is the number of particles and a is the hard-core diameter. Diamonds show the dependence when N is fixed ($N=128$) and a is varied, $4.33\times10^{-3}<a/a_{ho}<1.11$. Circles show the dependence when a is fixed $[a/a_{ho}=8(a_{Rb}/a_{ho})\approx0.035]$ and N is varied, $32\leqslant N\leqslant1024$. The short-dashed and long-dashed lines are linear and spline fits to the fixed a and fixed N data, respectively.

We have defined the radius of the ground state R_{QMC} by setting a cutoff value of the QMC number density $n(r)$ so that $n(R_{QMC})=10^{-5}$. Figure 8 shows QMC results for the dependence of the width R/a_{ho} of the ground-state density of N hard-core bosons on the product $(Na/a_{ho})^{1/5}$. In the figure, diamonds show the dependence when the number of particles is fixed, $N=128$, and the hard-core diameter a is varied, $4.33\times10^{-3}<a/a_{ho}<1.11$. The dashed line is a spline fit to the fixed $N=128$ data to guide the eye. Circles show the dependence when the hard-core diameter is fixed, $a/a_{ho}=0.035$, and N is varied, $32\leqslant N\leqslant1024$. The dashed line is a linear least-squares fit to the fixed-a data with slope ≈0.52. In the region $1\lesssim(Na/a_{ho})^{1/5}\lesssim1.75$, both fixed-$a$ and fixed-N results have a linear dependence on $(Na/a_{ho})^{1/5}$ with the same slope. In the region where the dependence on $(Na/a_{ho})^{1/5}$ holds, the maximum density of the trapped bosons is range in the $10^{-6}\lesssim na^3\lesssim5\times10^{-3}$. For small values of (Na/a_{ho}), the $(Na/a_{ho})^{1/5}$ dependence is not expected to hold since even a single-particle noninteracting system has a finite width. The width of the many-body ground state is no longer linearly dependent on $(a/a_{ho})^{1/5}$ for values of $(Na/a_{ho})^{1/5}>1.75$. In this regime, the maximum trap density is $na^3\gtrsim5\times10^{-3}$ and $a/a_{ho}\gtrsim0.1$. The present DMC results indicate that for $a/a_{ho}\gtrsim0.1$, the width of the many-body ground state depends on a/a_{ho} as $R\propto(a/a_{ho})^{2/3}$ rather than $(a/a_{ho})^{1/5}$. Linear dependence on $N^{1/5}$ continues to hold up to the highest number of particles considered ($N=1024$).

2. The total density profile

Figure 9 shows the DMC density profiles for 128 hard-sphere trapped bosons for four values of the maximum trap density na^3. Frame (a) shows the radial density profile for $a/a_{ho}=8(a_{Rb}/a_{ho})=0.034\,64$. The maximum density of the trapped bosons in this system occurs at the center of the trap with $na^3\approx2.25\times10^{-4}$. This corresponds to a typical density observed in experiments in metastable He* [44,45]. Frame (b) shows results for $a/a_{ho}=32(a_{Rb}/a_{ho})=0.138\,56$ and maximum density $na^3\approx6\times10^{-3}$, which is comparable with densities found in ^{85}Rb experiments. In frame (c), $a/a_{ho}=64(a_{Rb}/a_{ho})=0.277\,12$. Here, local correlations in the density distribution near the center of the trap are readily apparent. Finally, frame (d) shows the density profile for $a/a_{ho}=256(a_{Rb}/a_{ho})=1.108\,4$. In this system, the hard-spheres appear to have solidified in the center of the trap. The $n(r)a^3$ for this system is only qualitatively correct as mixed estimator bias caused by the guiding function used is a factor here.

3. Comparison of DMC $n(r)$ and Thomas-Fermi $n_{TF}(r)$

In the so-called ''Thomas-Fermi'' (TF) approximate form of the Gross-Pitaevskii equation, the interaction term $g\propto Na$ in the GP equation is assumed to dominate the ''kinetic-energy'' or gradient term resulting in an analytically solvable form of the GP equation. The TF approximation is expected to be valid when Na is large, $Na\gg1$, the interaction density is low, $na^3\ll1$, and the ratio of the scattering length to the characteristic harmonic trap length is small, $a/a_{ho}\ll1$.

Figure 10 shows a comparison of the total density distribution calculated using DMC, $n_{DMC}(r)$, to the density predicted by the Thomas-Fermi approximation

$$n_{TF}(r)=[(15Na)^{2/5}-x^2]/8\pi Na. \tag{20}$$

The top frame (a) shows the density profile for $N=1024$ bosons with $a/a_{ho}=8a_{Rb}=0.034\,64$. Here, the TF and DMC results agree quite well. However, the TF result slightly overestimates the density near the center of the trap and fails to reproduce the low-density tail which occurs near the edge of the trapped cloud. Frame (b) shows $n(r)$ for $N=128$ and $a/a_{ho}=64a_{Rb}=0.277\,12$. Note that the product, Na/a_{ho}, (the only variable responsible for determining the shape of the TF and GP density profiles) is the same in both frames. Clearly, in the bottom frame, the TF approximation dramatically overestimates the density at the center of the trap and underestimates the width of the condensate.

D. Condensate fraction

Figure 11 shows the condensate fraction n_0 as a function of the density na^3 for $N=128$ trapped hard-sphere bosons. The n is the maximum number density which is at the center of the trap in the density range shown. The density was varied by changing the value of a/a_{ho}. The corresponding values of a/a_{ho} are shown on the top axis. Circles are the mean-field-Bogoliubov (MFB) result for a uniform dilute Bose gas integrated over the GP density in the Thomas-Fermi limit [58] obtained by solving

$$n_0=1-0.3798(N_0a/a_{ho})^{6/5}/N. \tag{21}$$

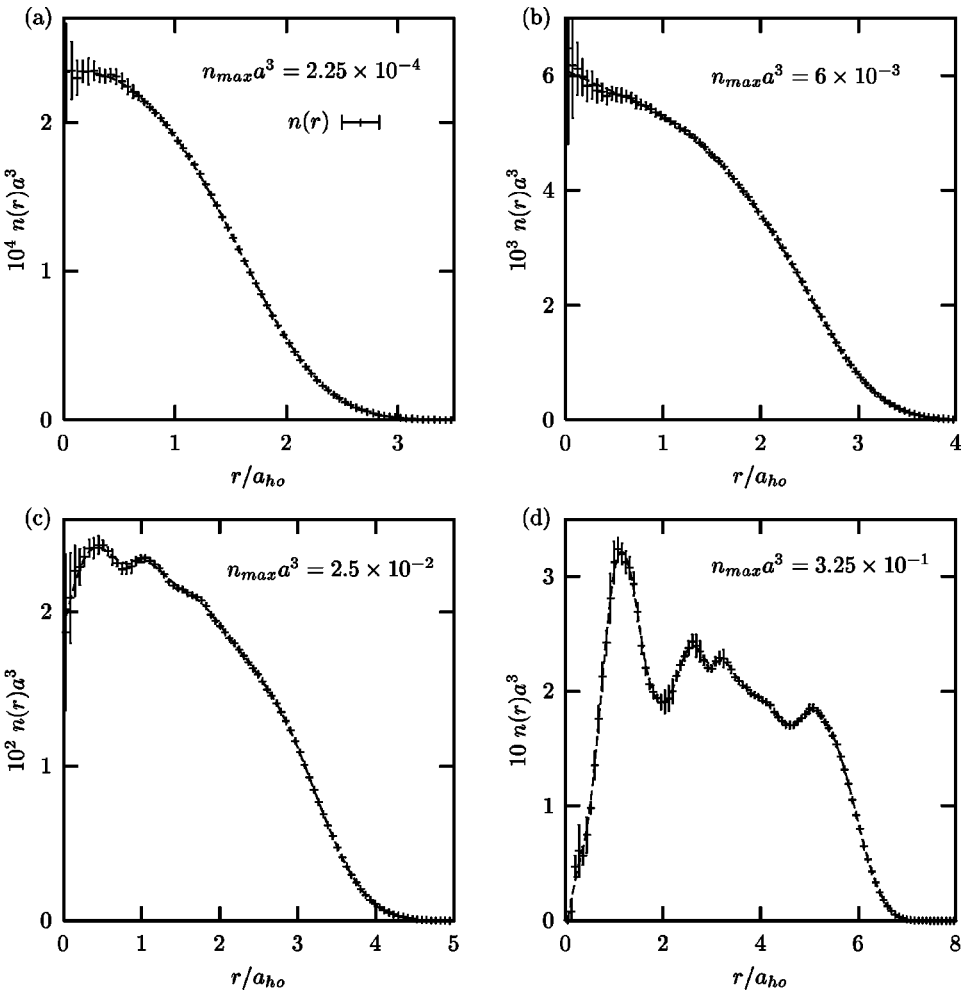

FIG. 9. DMC density profiles for hard-sphere trapped bosons for four values of the maximum trap density na^3. All plots are for $N=128$ and values of $a/a_{ho}=0.034\,64$, $0.138\,56$, $0.277\,12$, $1.108\,4$ for frames (a), (b), (c), and (d), respectively.

The up- and down-facing triangles are the DMC and VMC0 results, respectively, obtained from diagonalizing the OBDM. For $na^3<10^{-4}$, all three values of n_0 agree to within 1%. At higher densities, the MFB result consistently overestimates the condensate fraction. MFB overestimates the condensate fraction because it ignores local pair correlations which act to deplete the condensate. In contrast the DMC value of the condensate is consistently lower than either the VMC0 or MFB estimates. We believe that the DMC result for n_0 is lower than either VMC and MFB because it is able to treat local pair correlations more accurately. Pair correlations allow the total energy to decrease at the expense of long-range order. Since DMC is able to sample the exact ground state, the mixed estimate for n_0 obtained from DMC is more accurate than VMC or MFB.

Figure 12 shows n_0 over a wider density range. Here n is again the maximum number density in the trap. At high densities the maximum density in the trap is not always at the center of the trap. As in the dilute regime presented in Fig. 11, MFB consistently overestimates the condensate fraction for most densities. At $na^3\approx 0.28$, however, the MFB estimate of n_0 goes to zero while both VMC and DMC still show a condensate fraction of $n_0\approx 10\%$. The MFB estimate goes to zero because the TF density profile used to calculate the MFB value of n_0 does not have a broad low-density region near the surface of the trapped cloud of atoms as do the DMC and VMC density distributions. As will be shown in the following section, the dilute region at the ''edge'' of the trapped cloud can support a condensate even when the condensate fraction in the dense center of the trap goes to zero.

The density corresponding to liquid helium at SVP ($na^3=0.21$) is indicated on the plot. At this density, VMC gives a condensate fraction of $n_0\approx 25\%$ while DMC estimates a condensate fraction of $n_0\approx 18\%$. In bulk liquid ^{4}He, the condensate fraction is $n_0\approx 7.25\%$ [8]. This difference is explained by the fact that the dilute region near the surface of the trapped cloud allows for a larger fraction of particles to occupy the condensate orbital than in an uniform system at ^{4}He densities.

Table I summarizes the present DMC and VMC results for the condensate fraction over a wide density range.

E. Spatially dependent depletion of the condensate

In Fig. 13 we compare the total density distribution $n(r)$ to the condensate distribution, $n_0(r)=n_0|\phi_0(r)|^2$, for $N=128$ hard-sphere bosons in a harmonic trap calculated using diffusion Monte Carlo. In the top frame, $a/a_{ho}=64(a_{Rb}/a_{ho})$ giving a maximum density in the trap of $na^3\approx 2.4\times 10^{-2}$ and total condensate fraction of $n_0\approx 70\%$. In this system, the spatial distribution of the condensate fol-

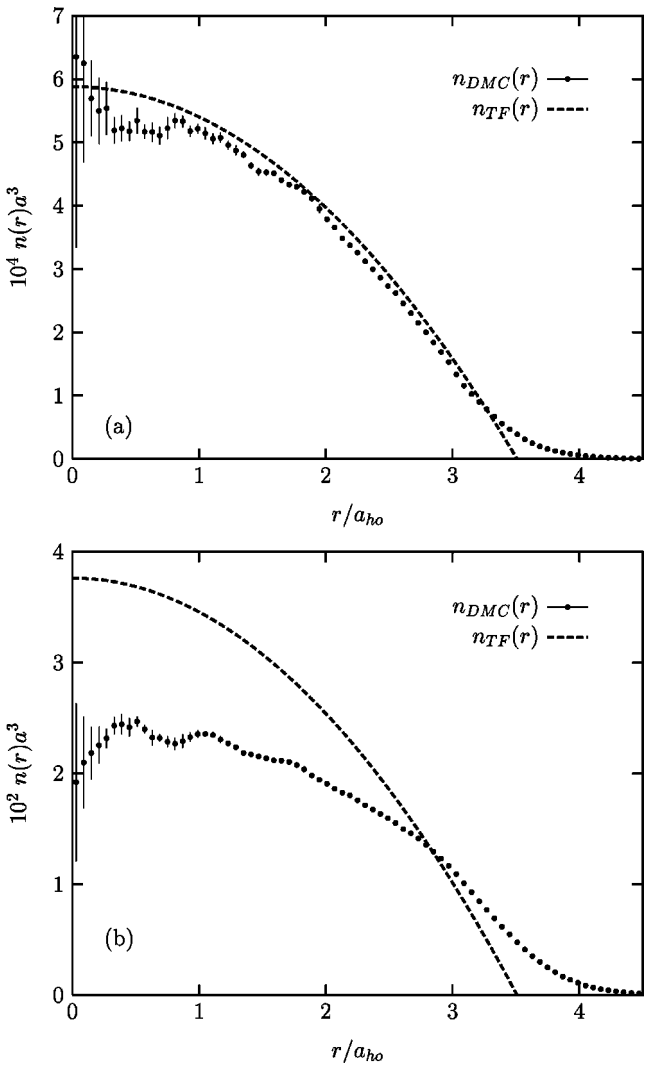

FIG. 10. Comparison of total density distribution calculated using diffusion Monte Carlo, $n_{\mathrm{DMC}}(r)$, for hard-sphere bosons in a harmonic trap to the density predicted by the Thomas-Fermi approximation (20). Top frame (a) is for $N=1024$ bosons with a ratio of scattering length to trap length of $a/a_{ho}=8a_{Rb}=0.034\,64$. Density is expressed in terms of $n(r)a^3\times10^4$. Frame (b) is for $N=128$ bosons with $a/a_{ho}=64a_{Rb}=0.277\,12$. Density is expressed in terms of $n(r)a^3\times10^2$.

lows the shape of the total density distribution except at small r. It is worth noting that while the total density exhibits local correlations in the dense region near the center of the trap, the condensate distribution is relatively flat in this region. In the bottom frame of the figure, $a/a_{ho}=256(a_{Rb}/a_{ho})=1.1084$ resulting in a maximum density of $na^3\approx0.325$ and a condensate fraction of $n_0\approx10\%$. This is the same system shown in frame (d) of Fig. 9. As discussed above, the DMC results at this density are biased by the VMC guiding function used. Nevertheless, we believe the results to be qualitatively correct. Here, strong pair correlations have completely depleted the condensate in the center of the trap but the relatively dilute region near the edge of the trap is still able to support a condensate. We find that for trapped hard-sphere bosons, the local condensate fraction

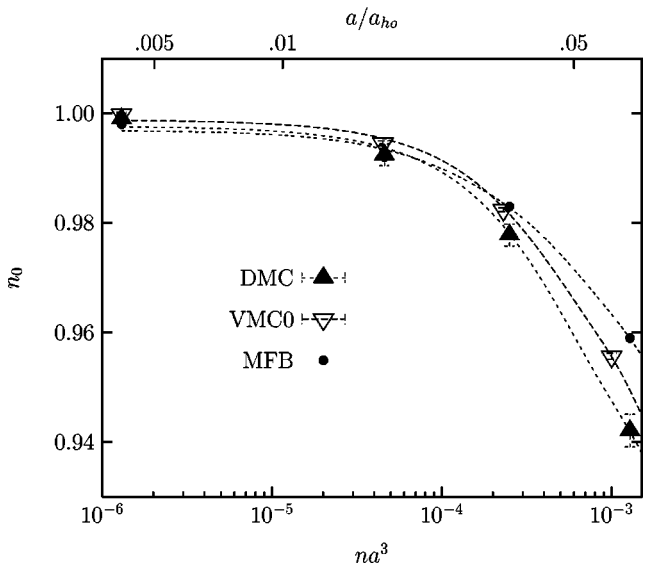

FIG. 11. Condensate fraction n_0 as a function of the density na^3 for $N=128$ trapped hard-sphere bosons. Here n is the number density at the center of the trap and a is the scattering length. Circles are from the mean-field Bogoliubov (MFB) expression for n_0 in a uniform dilute Bose gas integrated over the TF density. The up- and down-facing triangles are the DMC and VMC results, respectively. Dashed lines are spline fits to guide the eye.

$n_0(r)/n(r)$ rises in the dilute region near the surface and remains close to one all the way to the surface of the cloud. This may be contrasted with predictions for $n_0(r)/n(r)$ for self-bound superfluid ^{4}He at a free surface in which surface correlations significantly deplete the condensate at the liquid-vacuum interface [27,33].

IV. DISCUSSION

The main objectives of this work are to explore the role of interactions in determining the zero-temperature properties

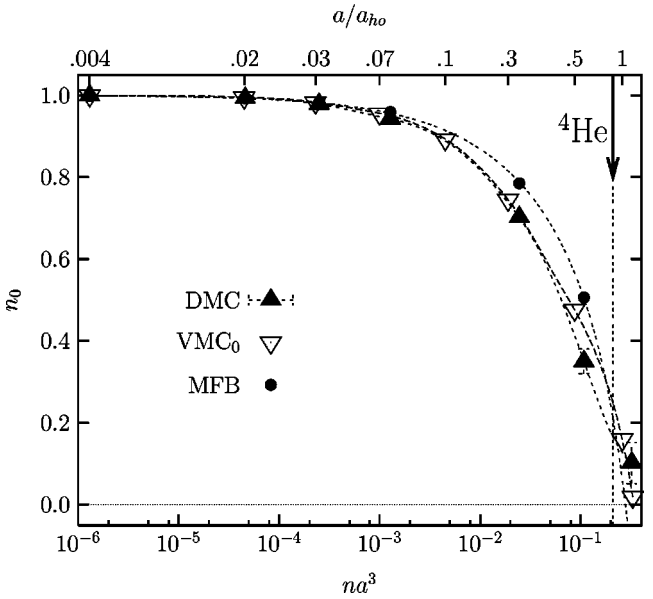

FIG. 12. Condensate fraction n_0 over a wide density range. The legend is the same as Fig. 11.

TABLE I. Condensate fraction as obtained from mean-field-Bogoliubov (MFB) , VMC, and DMC methods.

na^3	a/a_{ho}	MFB	VMC	DMC
1.3×10^{-6}	1	0.998	0.999(9)	0.99(9)
4.6×10^{-5}	4	0.992	0.992(4)	0.99(2)
2.5×10^{-4}	8	0.983	0.977(8)	0.97(7)
2.5×10^{-3}	16	0.959	0.942(1)	0.94(2)
2.4×10^{-2}	64	0.785	0.745(7)	0.70(2)
1.1×10^{-1}	128	0.506	0.476(5)	0.3(5)
3.2×10^{-1}	256	*N/A*	0.160(0)	0.1(0)

[a]MFB predicts a negative condensate fraction for this system.

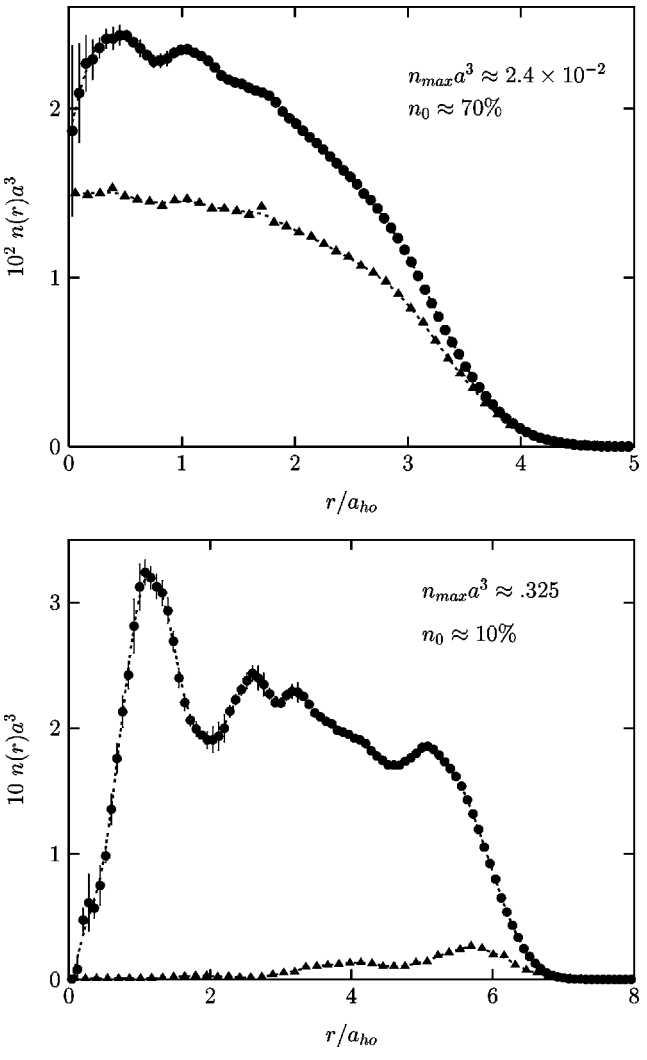

FIG. 13. Comparison of total density distribution $n(r)$ to condensate distribution, $n_0(r)=|\phi(r)|^2$, for $N=128$ hard-sphere bosons in a harmonic trap calculated using diffusion Monte Carlo. Circles are the total density while triangles represent the condensate. Dashed lines are spline fits to guide the eye. In the top frame, the maximum density in the trap is $na^3\approx2.4\times10^{-2}$ and the total condensate fraction is $n_0\approx70\%$. In the bottom frame, $na^3\approx2.4\times10^{-2}$ and $n_0\approx10\%$.

of the trapped Bose gas over a wide range of densities and to determine the limits of the mean-field description of the condensate properties. To this end, we have employed QMC methods and the OBDM formulation of BEC. We find the OBDM description of a many-body Bose system combined with QMC techniques provides a coherent method for the study of the ground-state properties and Bose-Einstein condensation in traps from the dilute to the very dense regime. By comparing our QMC results with mean-field theory we determine key limits of the mean-field description.

A. The ground-state energy

We find that in the dilute limit, $na^3\lesssim10^{-4}$, where the condensate depletion is small, $n_0\gtrsim99\%$, the GP description of the condensate provides a good description of the full many-body ground state. Once the density has reached, $na^3\approx10^{-3}$, $\approx6\%$ of the atoms lie outside of the condensate and the condensate energy obtained from GP theory lies 3% below the QMC energy. For $na^3\gtrsim10^{-3}$, the GP energy does not describe the energy of the bosons in the trap accurately. The present QMC corrections to the GP energy, $\delta E=E_{DMC}-E_{GP}$, are proportional to $N^{3/5}$ when N is allowed to vary with fixed a and are proportional to $(a/a_{ho})^{8/5}$ when a is allowed to vary with fixed N. This dependence on N and a holds for all densities studied ($10^{-6}<na^3<0.5$) and is consistent with the expected corrections to the GP energy arising from the depletion of condensate (18). Thus, the GP description of the condensate energy appears to be valid even in the highly interacting regime. However, the dependence of δE on the product $N^{3/5}(a/a_{ho})^{8/5}$, as predicted by MGP (18), holds up to densities $na^3\approx5\times10^{-4}$ only. As interaction is increased the effects of the noncondensate play an increasingly significant roll in determining the properties of the total ground state and a more complicated functional dependence of $\delta E(N,a)$ than the simple product $N^{3/5}(a/a_{ho})^{8/5}$ is required at higher densities.

B. Deviations from the mean-field description

Figure 14 contains striped bands indicating regions in a/a_{ho} where QMC results diverge from mean-field / Bogoliubov predictions. Since the degree of depletion of the condensate arising from interboson interaction plays a significant role in determining beyond-mean-field effects, QMC values for the number of atoms outside the condensate, $\tilde{N}$, for a system with a total of $N=128$ bosons are shown along with the regions. The first sign of divergence (a) occurs at a density of $na^3\approx3\times10^{-4}$ and a value of $a/a_{ho}\approx8(a_{Rb}/a_{ho})\approx0.035$. At this density, QMC and MFB (21) results for the condensate fraction, $n_0=N_0/N$, begin to diverge (see Fig. 11). Below this value of a/a_{ho}, QMC and MFB values of n_0 agree to within 1%. At $na^3\approx10^{-3}$, MFB underestimates the depletion of the condensate by 30%. At higher densities, $na^3\approx10^{-1}$, MFB predicts a condensate fraction 40% higher than QMC.

The second point of interest in Fig. 14 marked (b) occurs in the region of $na^3\approx2.5\times10^{-3}$ and $a/a_{ho}\approx0.12$. Near this value of a/a_{ho}, QMC results for the size of the many-body

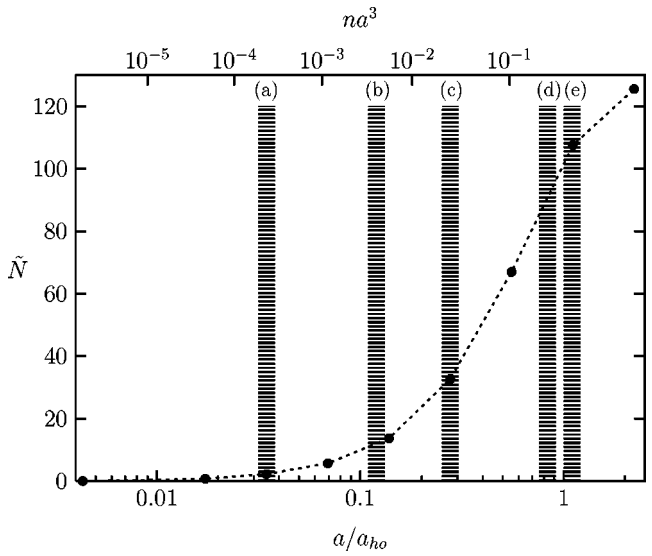

FIG. 14. QMC determination of the number of bosons outside the condensate, $\tilde{N}$, for $N=128$ hard-sphere bosons in a spherically symmetric harmonic trap vs a/a_{ho}. The corresponding densities na^3 are shown across the top axis. Striped bands indicate regions in a/a_{ho} where the QMC results for BEC properties diverge from mean-field / Bogoliubov predictions. (a) QMC and Bogoliubov results for n_0 begin to diverge. (b) QMC and mean-field results for the size of the condensate diverge. (c) Local correlations in the density profile of the many-body ground state begin to appear. (d) The condensate begins to shift from the center of the trap. (e) The condensate exists only in the dilute region near the surface of the trapped cloud.

ground-state and mean-field results for the size of condensate (19) begin to differ. For values of $a/a_{ho} \lesssim 0.12$, the width of the many-body ground state is proportional to $(Na/a_{ho})^{1/5}$ as predicted by mean-field theory. At higher values, $(a/a_{ho} > 0.12)$, we find that the size of the condensate is better described by a scaling of $(a/a_{ho})^{2/3}$. The scaling is shown in Fig. 8 and discussed in Sec. III C 1. Thus, for systems with $na^3 \gtrsim 10^{-3}$, GP theory in the TF limit underestimates the growth of the size of the ground state with a/a_{ho} significantly. In the extreme range of very large scattering length or very tight trapping potential where $a/a_{ho}=1$, GP predicts a condensate distribution 20% smaller than the width of the ground state obtained from QMC.

Band (c) in Fig. 14 indicates the region in which local correlations in the density profile of the many-body ground state begin to appear. These local correlations signal a clear departure from mean-field properties. This effect occurs for systems with trap densities of $na^3 \gtrsim 2.5\times 10^{-2}$ and $a/a_{ho} \approx 64(a_{Rb}/a_{ho}) \approx 0.28$. At this level of interaction the condensate fraction as obtained from DMC is $n_0 \approx 70\%$. We find that at this density the condensate density is smoothly varying throughout the trap with little or no local-density fluctuations (see top frame of Fig. 13). Evidence that the condensate distribution does not explicitly follow the total density distribution is another demonstration that a local-density approximation description of the condensate breaks down at this density.

The band marked (d) in Fig. 14 approximates the region in which the condensate begins to shift from the center of the trap to the surface. Here, $na^3 \approx 0.2$ and $a/a_{ho} \approx 0.8$. The condensate fraction is $n_0 \approx 20\%$. At this level of interaction and beyond, mean-field approximations and the Bogoliubov approximation both fail to appropriately describe the properties of a trapped BEC. We speculate that at this density, the increased depletion in the center of the trap could effectively pin vortex states.

The final point of interest in Fig. 14 occurs in the region marked by the band (e). For systems with $na^3 \gtrsim 0.3$ and $a/a_{ho} \gtrsim 256(a_{Rb}/a_{ho}) \approx 1.1$, the condensate exists only in the dilute region near the surface of the trapped cloud. Strong pair correlations have completely depleted the condensate in the center of the trap but the relatively dilute region near the edge of the trap is still able to support a condensate. Figure 13 presents DMC results which demonstrate this phenomena.

ACKNOWLEDGMENTS

Stimulating discussions with J. Boronat and S. A. Chin as well as comments on the original manuscript from D. Blume are gratefully acknowledged. Partial support from National Science Foundation (Grant No. DMR-0115663) is gratefully acknowledged.

[1] A. Einstein, Sitzungsber. Preuss. Akad. Wiss., Phys. Math. Kl. **1925**, 3 (1925).
[2] S. Bose, Z. Phys. **26**, 178 (1924).
[3] F. London, Phys. Rev. **54**, 947 (1938).
[4] F. London, Nature (London) **141**, 643 (1938).
[5] A.J. Leggett, Rev. Mod. Phys. **73**, 307 (2001).
[6] D.M. Ceperley, Rev. Mod. Phys. **67**, 279 (1995).
[7] S. Moroni, G. Senatore, and S. Fantoni, Phys. Rev. B **55**, 1040 (1997).
[8] H.R. Glyde, R.T. Azuah, and W.G. Stirling, Phys. Rev. B **62**, 14 337 (2000).
[9] N. Bogoliubov, J. Phys. (USSR) **11**, 23 (1947).
[10] L. Onsager and O. Penrose, Phys. Rev. **104**, 576 (1956).
[11] P.O. Löwdin, Phys. Rev. **37**, 1474 (1955).
[12] M.H. Anderson, J.R. Ensher, M.R. Matthews, C.E. Wieman, and E.A. Cornell, Science **269**, 198 (1995).
[13] K.B. Davis, M.-O. Mewes, and W. Ketterle, Appl. Phys. B: Lasers Opt. **B60**, 155 (1995).
[14] C.C. Bradley, C.A. Sackett, J.J. Tollett, and R.G. Hulet, Phys. Rev. Lett. **75**, 1687 (1995); **79**, 1170 (1997).
[15] F. Dalfovo, S. Giorgini, L.P. Pitaevskii, and S. Stringari, Rev. Mod. Phys. **71**, 463 (1999).
[16] W. Krauth, Phys. Rev. Lett. **77**, 3695 (1996).
[17] K. Ziegler and A. Shukla, Phys. Rev. A **56**, 1438 (1997).
[18] E. Timmermans, P. Tommasini, and K. Huang, Phys. Rev. A **55**, 3645 (1997).
[19] E. Braaten and A. Nieto, Phys. Rev. B **56**, 14 745 (1997).
[20] P. Grüter, D.M. Ceperley, and F. Laloë, Phys. Rev. Lett. **79**,

3549 (1997).
[21] S. Pearson, T. Pang, and C. Chen, Phys. Rev. A **58**, 4811 (1998).
[22] M. Holzmann and W. Krauth, Phys. Rev. Lett. **83**, 2687 (1999).
[23] D.A. Hutchinson, Phys. Rev. Lett. **82**, 6 (1999).
[24] A. Fabrocini and A. Polls, Phys. Rev. A **60**, 2319 (1999).
[25] S. Giorgini, J. Boronat, and J. Casulleras, Phys. Rev. A **60**, 5129 (1999).
[26] B. Tanatar and K. Erkan, Phys. Rev. A **62**, 053601 (2000).
[27] D.E. Galli and L. Reatto, J. Phys.: Condens. Matter **12**, 6009 (2000).
[28] D. Blume and C.H. Greene, Phys. Rev. A **63**, 063601 (2001).
[29] A. Fabrocini and A. Polls, Phys. Rev. A **64**, 063610 (2001).
[30] A. Banerjee and M.P. Singh, Phys. Rev. A **64**, 063604 (2001).
[31] G.E. Astrakharchik, J. Boronat, J. Casulleras, and S. Giorgini, Phys. Rev. A **66**, 023603 (2002).
[32] A.Y. Cherny and A.A. Shanenko, Phys. Lett. A **293**, 287 (2002).
[33] E.W. Draeger and D.M. Ceperley, Phys. Rev. Lett. **89**, 015301 (2002).
[34] J.O. Andersen and H. Haugerud, Phys. Rev. A **65**, 033615 (2002).
[35] C.G. Bao, Y.Z. He, G.M. Huang, and T.Y. Shi, Phys. Rev. A **65**, 022508 (2002).
[36] D. Blume, Phys. Rev. A **66**, 053613 (2002).
[37] G.E. Astrakharchik and S. Giorgini, Phys. Rev. A **66**, 053614 (2002).
[38] S. Inouye, M.R. Andrews, J. Stenger, H.-J. Miesner, D.M. Stamper-Kurn, and W. Ketterle, Nature (London) **392**, 151 (1998).
[39] J. Stenger, S. Inouye, M.R. Andrews, H.-J. Miesner, D.M. Stamper-Kurn, and W. Ketterle, Phys. Rev. Lett. **82**, 2422 (1999).
[40] S.L. Cornish, N.R. Claussen, J.L. Roberts, E.A. Cornell, and C.E. Wieman, Phys. Rev. Lett. **85**, 1795 (2000).
[41] J.L. Roberts, J.P. Burke, Jr., N.R. Claussen, S.L. Cornish, E.A. Donley, and C.E. Wieman, Phys. Rev. A **64**, 024702 (2001).
[42] J.L. Roberts, Ph.D. thesis, University of Colorado.
[43] T. Weber, J. Herbig, M. Mark, H.C. Nagerl, and R. Grimm, Science **299**, 232 (2003).
[44] A. Robert, O. Sirjean, A. Browaeys, J. Poupard, S. Nowak, D. Boiron, C.I. Westbrook, and A. Aspect, Science **292**, 461 (2001).
[45] F.P.D. Santos, J. Leonard, J.M. Wang, C.J. Barrelet, F. Perales, E. Rasel, C.S. Unnikrishnan, M. Leduc, and C. Cohen-Tannoudji, Phys. Rev. Lett. **86**, 3459 (2001).
[46] C. I. Westbrook, A. Robert, O. Sirjean, A. Browaeys, D. Boiron, and A. Aspect, in *Laser Spectroscopy*, Proceedings of the XV International Conference, edited by S. Chu, V. Vuletic, A. Kerman, and C. Chin (World Scientific, Singapore, 2002), p. 2.
[47] D.G. Fried, T.C. Killian, L. Willmann, D. Landhuis, S.C. Moss, D. Kleppner, and T.J. Greytak, Phys. Rev. Lett. **81**, 3811 (1998).
[48] M.H. Kalos, D. Levesque, and L. Verlet, Phys. Rev. A **9**, 2178 (1974).
[49] F. Dalfovo and S. Stringari, J. Chem. Phys. **115**, 10 078 (2001).
[50] J.L. DuBois and H.R. Glyde, Phys. Rev. A **63**, 023602 (2001).
[51] S.A. Chin, J. Low Temp. Phys. **93**, 921 (1993).
[52] J.D. Reppy, B.C. Crooker, B. Hebral, A.D. Corwin, J. He, and G.M. Zassenhaus, Phys. Rev. Lett. **84**, 2060 (2000).
[53] J. Wilks, *The Properties of Liquid and Solid Helium* (Clarendon Press, Oxford, 1967).
[54] E.L. Pollock and K.J. Runge, Phys. Rev. B **46**, 3535 (1992).
[55] P.J. Reynolds, D.M. Ceperley, B.J. Alder, and W.A. Lester, J. Chem. Phys. **77**, 5593 (1982).
[56] J. Casulleras and J. Boronat, Phys. Rev. B **52**, 3654 (1995).
[57] G. Baym, *Lectures on Quantum Mechanics* (Benjamin, New York, 1976), p. 425.
[58] J. Javanainen, Phys. Rev. A **54**, R3722 (1996).